Audio Engineering Society

Convention Paper

Presented at the 125th Convention
2008 October 2–5 San Francisco, CA, USA

Confirmation of chaos in a loudspeaker system using time series analysis

Joshua D. Reiss[1], Ivan Djurek[2], Antonio Petosic[2] and Danijel Djurek[3]
[1] Centre for Digital Music, Queen Mary, University of London, Mile End Road, London, E14NS, U. K.
josh.reiss@elec.qmul.ac.uk

[2] University of Zagreb, Faculty of Electrical Engineering and Computing, Dept. of Electroacoustics
Unska 3, Zagreb, Croatia
ivan.djurek@zg.t-com.hr; antonio.petosic@fer.hr

[3] AVAC – Alessandro Volta Applied Ceramics, Laboratory for Nonlinear Dynamics
Kesten brijeg 5, Remete, Zagreb, Croatia
danijel.djurek@zg.t-com.hr

ABSTRACT

The dynamics of an experimental electrodynamic loudspeaker is studied by using the tools of chaos theory and time series analysis. Delay time, embedding dimension, fractal dimension and other empirical quantities are determined from experimental data. Particular attention is paid to issues of stationarity in the system in order to identify sources of uncertainty. Lyapunov exponents and fractal dimension are measured using several independent techniques. Results are compared in order to establish independent confirmation of low dimensional dynamics and a positive dominant Lyapunov exponent. We thus show that the loudspeaker may function as a chaotic system suitable for low dimensional modeling and the application of chaos control techniques.

1. INTRODUCTION

Loudspeakers are the most variable elements in any audio system, and are responsible for marked audible differences between otherwise identical sound systems. Loudspeaker performance (i.e., their accuracy in reproducing a signal without adding distortion) is significantly poorer than that of other audio equipment. For example, harmonic distortion in a typical loudspeaker can be 100 to 1000 times greater than that of amplifiers[1]. The frequency response of a loudspeaker is often referenced as being within ±3 dB of perfect linearity (and many speaker designs fall further outside this range), whereas an amplifier may vary less than 0.1 dB.

An electrodynamic loudspeaker consists of a membrane suspended to a fixed rim and put in motion by the

Lorentz force exerted on the voice coil positioned in the field of a permanent magnet. The Lorentz force oscillates in the same phase and frequency as the current generated by the sound radiation, and it is commonly accepted that the membrane vibrates with amplitude being linearly dependent on the amplitude of the input AC signal, while natural frequency is expected to be independent of vibration amplitude, i.e. the system operates in a linear regime. However, this is true only for small driving AC currents (<10 mA). For higher currents the vibration amplitude deviates from the linear dependence and natural frequency changes with changing amplitude of the input signal.

It is of great importance to study such a nonlinear system in terms of the laws and rules of widely quoted nonlinear phenomena, including stability theories. Their development makes possible the use of new physical tools in understanding the loudspeaker vibration properties. Thus an improved understanding of the dynamics of a loudspeaker is of great importance, since when taking into account the nonlinear phenomena, a loudspeaker might be better designed and yield significantly better performance in an audio playback system.

Evidence of possible chaotic behavior in a loudspeaker was first observed by Wei, et al in 1986[2], where the appearance of subharmonics and broadband spectra at various drive frequencies and voltages was noted. Tong, et al[3] also identified chaos through the measurement of Lyapunov exponents and fractal dimension, although their results were not held up to scrutiny and may be considered unreliable (for instance, they do not report how many data points were used and the results are not repeatable). Recent work strengthened the conjecture of chaotic behavior [4-6] with the observation of hysteresis, also reported in [7], and period doubling when the loudspeaker is driven at low frequencies. This in general is not observed in the models and thus it is important to verify chaos and adjust the models accordingly.

The question arises whether study of the chaotic state may be useful in the construction of the loudspeaker. It was found[6] that chaos appears in loudspeakers with comparatively high intrinsic friction (R_i ~ 0.6-0.7 kg/sec measured at driving current I_0 = 10-100 mA), as evaluated from the resonance line width. This should be compared to a non-chaotic loudspeaker with R_i ~ 0.17-0.20 kg/sec, and high intrinsic friction would normally be an indication of the poor quality of the loudspeaker. However, resonance line width by itself does not necessarily imply a reduction of the harmonic nature of the loudspeaker, when considered as a forced oscillator. Of primary importance is the dependence of the intrinsic friction on the vibration amplitude. This dependence contributes to the temperature rise on the membrane surface. This is low in high quality loudspeakers, due to the high heat capacity of the membrane material. The temperature rise in turn reduces the thermo-elastic noise in the membrane and contributes to the quality of sound reproduction.

A dynamical system is represented by a set of nonlinear equations[8, 9] given in the form

$$\frac{d\psi_i}{dt} = F_i\left(\psi_1 \cdots \psi_2\right) \qquad i = 1,..,N \tag{1}$$

which might be applied to a nonlinear forced oscillator described by the equation of motion

$$\begin{aligned} &a\frac{d^2x}{dt^2} + b\frac{dx}{dt} + k\cdot x = f_1 = f_0\cdot\cos\phi \\ &\phi = \psi_2 = \omega t,\ \psi_1 = \frac{dx}{dt} \end{aligned} \tag{2}$$

In the linear regime when the electrodynamic loudspeaker (EDL) is driven by a small current (I_0~10 mA), the coefficients in equation (2) are nearly constant, and stiffness k is expressed by the natural frequency ω_0 and mass M in the form $k=\omega_0^2 M$. The solution to equation (2) can be expressed as $x=A\cdot\cos\omega t$.

In this form, displacement x in equation (2) properly describes only the motion of the voice coil, while the points on the membrane, because of its flexibility, suffer combined displacement $x+z$, z being the solution of the Bessel equation which is given in the radial coordinate r

$$\rho\cdot\frac{d^2z}{dt^2} + E\cdot\Delta z = \rho\frac{d^2z}{dt^2} - E\left(\frac{d^2z}{dr^2} + \frac{1}{r}\frac{dz}{dr}\right) = f_2 \tag{3}$$

E and ρ are the Young modulus and density of the membrane polymeric material, respectively. Equation (3) expresses force density coming from the inertial and elastic shear term. After integration over the membrane volume both terms can be added to the left side of equation (2).

However, the Bessel modes derived from equation (3) do not contribute to the intrinsic friction of the membrane, but such a friction results from the viscoelastic losses and these losses are manifested by

fluctuations in the membrane surface visible as tilts[10]. Such tilts are stochastic surface fluctuations and are associated to vibration modes having frequencies extending up two orders of magnitude higher than loudspeaker's natural frequency.

In these experiments, stiffness k was evaluated from the static measurements by the use of calibrated loads and the evaluation of corresponding membrane displacements. It was found that stiffness has a form $k=m+n\cdot x+p\cdot x^2$ ($m = 930$ Nm^{-1}, $n = -114\cdot10^3$ Nm^{-2}, $p = 32\cdot10^3$ Nm^{-3}), and k obtains a minimum value at x~1.8 mm. A short analysis of equation (2) shows that it would be exceedingly difficult to explain amplitude bifurcations and the existence of a chaotic state in the loudspeaker by this nonlinearity, even if coefficients m, n, and p are varied over a broad range of values far from the commonly accepted values indicated by the technical performance of the loudspeaker. Instead, the only effect observed by the use of simulations based upon this quadratic nonlinearity was the well known amplitude cut-off[11], as shown in the inset of Figure 1.

Another experiment showed that the membrane's properties play an important role in the dynamics of the system. The same membrane was reinforced by phenolic resin[12], leaving the elastic suspension intact. Static measurement of the stiffness after the reinforcement revealed that k increased to about 1230 Nm^{-1} at the origin, and this is to be contrasted with the concept of the EDL membrane as being a point mass suspended on an elastic spring. Furthermore, an increase of the stiffness by such reinforcement suggests a substantial contribution of membrane elasticity to the vibration properties of the EDL.

In addition to the elastic properties of the membrane governed by the Young modulus, viscoelasticity of the composite polymer material also plays an important role. Viscoelastic losses in the membrane are expressed by intrinsic membrane friction R_i entering the second term in equation (2), and these losses are brought about as a hysteresis in the stress-strain diagram of the membrane material. Systems with such hysteresis obey memory properties which manifest in the loudspeaker as a time dependent stiffness[13], and in the literature dealing with stochastic processes are commonly referred as an *after effect*.

Furthermore, one has to consider that a resonance frequency dependent on vibration amplitude (Figure 2) deviates from the dependence of the resonance frequency calculated from the formula $k=\omega_0^2\cdot M$, k being measured statically by the use of the calibrated loads. An initial decrease of the calculated resonance frequency from static measurements correlates to a decrease of the resonant frequency obtained from dynamic measurements, but a strong increase of the latter at A>5 mm might not be explained bythe simple quadratic nonlinearity in equation (2). Properties of the membrane material also play an important role in the restoring force.

In this respect, investigation of the dynamics of the chaotic state can provide very useful information concerning the composition and elastic properties of the membrane. This, in turn, could enable important improvements to the membrane design.

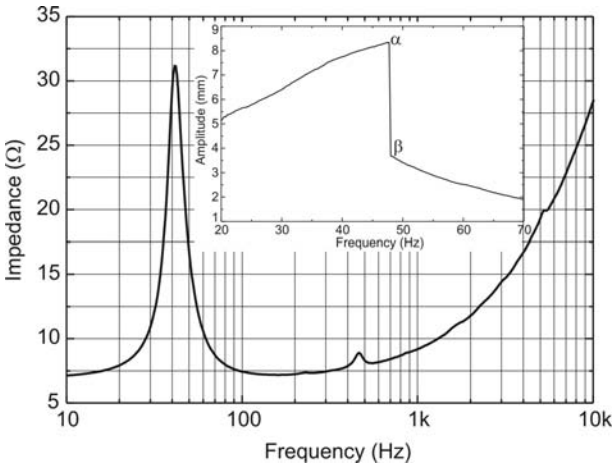

Figure 1. Frequency dependence of the impedance of the loudspeaker. The inset shows the frequency dependence of the vibration amplitude for driving current I0=4 A.

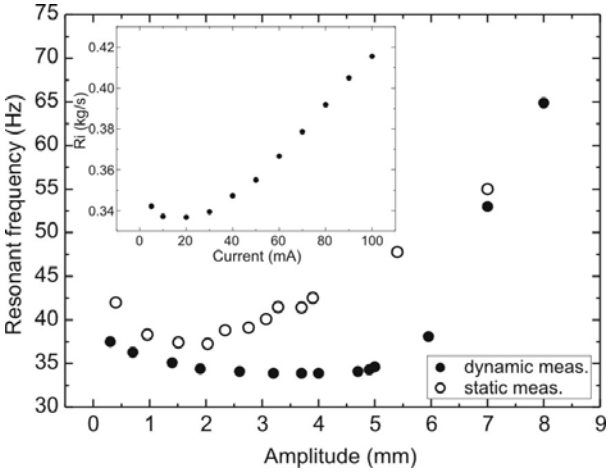

Figure 2. Amplitude dependent resonant frequency; (○) calculated from the statically measured stiffness, (●) measured in dynamic regime. Inset shows current dependent intrinsic membrane friction R_i.

In this work, we analyze time series from an experimental electrodynamic loudspeaker system. We use a variety of techniques from chaotic time series analysis[14] to show that the system is indeed chaotic and exhibits low dimensional dynamics suitable for further analysis and the implementation of chaos control techniques. By quantifying the nonlinear behavior, we also provide empirical observations which may be used to refine the modeling and design of loudspeakers.

2. EXPERIMENTAL SET-UP

In these experiments, a low frequency loudspeaker was used with a resonant frequency, recorded in air, of f = 38 Hz, driving current I_0 = 10 mA, factor $B{\cdot}l$ = 3.9 Tm, membrane diameter $2R$ = 16 cm, rated RMS power of 60 W, and nominal impedance of 8 ohms. According to the manufacturer's data, the voice coil inductance is L = 0.9 mH, and the contribution of the inductive part $\omega{\cdot}L$ to the loudspeaker's impedance can be neglected for driving frequencies f < 100 Hz.

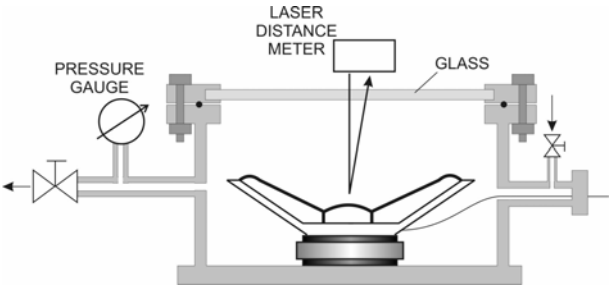

Figure 3. Experimental set up with loudspeaker and laser distance meter.

The experimental set-up is depicted in Figure 3. The loudspeaker was placed in a stainless steel chamber. Air pressure within the chamber was measured by the use of an absolute capacitive gauge with ultimate resolution 0.01 mbar. A glass window on the top of the chamber ensured the transparency to the light beam from the laser distance meter which measured vibration amplitude with an accuracy of 2 μm, and sampling frequency of ~ 1 kHz (a similar measurement apparatus was used to analyse nonlinear vibrations of a loudspeaker in Wei, et al[2]). The A/D converter resolution of the laser distance meter was 8 bits. This allowed the acquisition of 128 amplitude levels in both up and down vibration directions. In order to check the possible influence of the chamber wall friction on the course of measurements, the impedance and vibration amplitude data were recorded at 1 bar air pressure in closed chamber and compared to those evaluated in free laboratory atmosphere. In the frequency range near 50 Hz recorded data, notably impedance, showed no significant difference.

For impedance and amplitude measurements, the loudspeaker was connected to an audio amplifier with rated power of 300W via a series resistor 0.44 Ω. A rather small resistor value was used because of the possibility of driving higher currents. However, small resistance gave rise to increased influence of the back electromotive force. A satisfactory compromise was found with the total voltage swing across the loudspeaker, clipping not included, of +/- 50 V, which in turn provided driving currents I_0 = 4 to 5A. For driving currents I_0 < 100 mA, the back electromotive force is comparable to the friction term in Eq. (2), while for higher currents intrinsic friction increased and became the dominant contribution to the impedance.

The loudspeaker vibration amplitude dependent on frequency was measured for various driving currents in an evacuated space and in normal atmospheric pressure (1 bar)[15]. The data recorded *in vacuo* are shown in Figure 4. By an increase of the driving current the resonance curve became more and more distorted until an amplitude downturn (cut-off) appeared near f = 43.5 Hz for I_0 = 200 mA. This current indicated the starting value for identification of the chaotic regime. The inset in Figure 4 depicts the hysteretic property of the cut-off effect. That is, cut-off frequencies differ for positive and negative frequency sweep.

Onset of the amplitude cut-off was followed by a subsequent frequency sweep which gave rise to the erratic vibration amplitude. This unstable range extended up to 54 Hz. This was chosen as the fixed frequency for evaluation of the appearance of subharmonics which precede the chaotic state. An important feature of the unstable range was the relatively small change of the impedance with increasing driving current. In these experiments, loudspeaker impedance stayed at ~ 11 Ω, irrespective of whether the system was operated in air or in an evacuated chamber. This in turn meant that the driving system could be considered as a current source, even in the case when the amplifier was used as a voltage source.

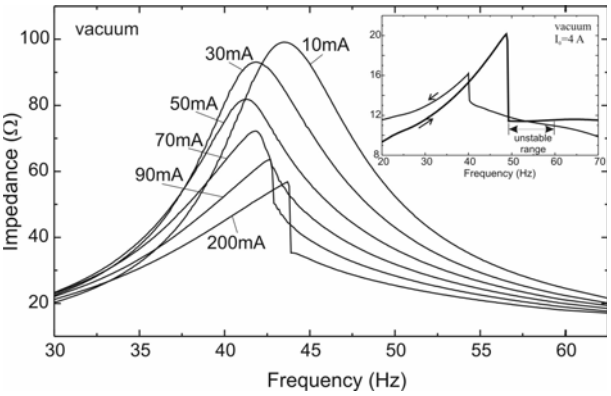

Figure 4. Impedance measured in vacuo for various driving currents. The inset shows the hysteresis of the cut-off frequency for positive and negative frequency sweeps.

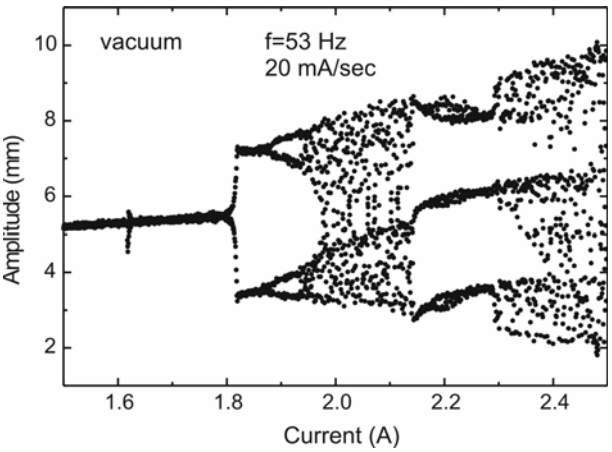

Figure 5. A bifurcation diagram of vibration amplitudes recorded in vacuo for fixed driving frequency 53 Hz and 20 mA/sec sweeping driving current.

A bifurcation diagram, as shown in Figure 5, was produced by fixing the frequency at f = 53 Hz, sweeping the driving current from I_0 = 1.5 A to 2.5A at a rate of 20 mA/sec, and recording the amplitude of the displacement of the loudspeaker. At I_0 ~ 1.81, a first bifurcation pitchfork appeared, which was followed by multiple period doublings, until at I_0 = 2.15 A the characteristic period-3 window appeared[16] and the system vibrated with 3 amplitudes. Existence of period doubling and a period 3 window was a strong indicator of chaos.

However, the period 3 window was observed only in an evacuated space, and data from a loudspeaker operating in an evacuated chamber is unsuitable for time series analysis techniques. This is primarily because the voice coil bonding agent evaporates when in a vacuum, which in turn changes the resonant frequency during the course of the measurements. In addition, for long time and heavy duty loudspeaker operation it is important to remove heat from the loaded voice coil, and this is more easily accomplished in an air atmosphere.

Measurements in 1 bar air were performed in a closed chamber, since this minimised parameter drift due to free air convection in the laboratory. The driving frequency was fixed at 56 Hz, and the driving current was increased up to values when higher harmonics appeared as a result of the nonlinear restoring term in Eq. (2). Excerpts of the time series waveforms representing various driving currents are given in Figure 6. Figure 6a shows the time dependent vibration amplitude at the starting driving current I_0 = 2.4 A, when the recorded signal shows nearly sinusoidal behavior. Figure 6b, c and d show new vibration amplitudes (marked with triangles) which appear with increasing driving current. The corresponding averaged spectra over the whole time series given in Figure 7. Figure 7a shows the expected behavior, with a fundamental frequency corresponding to the drive frequency. The first subharmonic appeared at 28 Hz, as depicted in Figure 7b. Further increase of the driving current resulted in a new subharmonic at 14 Hz (see Figure 7c) and the subsequent appearance of broadband behavior, Figure 7d.

The bifurcation diagram for measurements of vibration amplitude in air is shown in Figure 8, and was produced in the same manner as Figure 5. Vertical lines indicate values of driving currents for which the Feigenbaum ratio δ_1/δ_2 = 4.669 is fulfilled[17]. A period 3 window cannot be seen, but this is not a contra-indicator of

chaos. Noise in the data acquisition system may obscure the window, and existence of such a window is not considered a necessary condition. Whereas heating the voice coil makes long term measurements difficult for the evacuated loudspeaker experiment, reverberation and air circulation added noise to the short term measurements used in generating the bifurcation diagram of Figure 8.

Leaving the loudspeaker to operate at a driving frequency of 45 Hz, the driving current was selected at a value slightly below 2.8 A, at which point the first subharmonic became attenuated. This indicated the starting point for recording the vibration amplitude included in time series analysis. A rather low frequency of 45 Hz was selected because the dynamics appeared less susceptible to parameter drift and nonstationary behaviour in this range.

The time series analysis presented in the following sections is derived from a 247,392 point experimental flow data set. The data was recorded with 16bit resolution, though this is further limited by the 8 bit resolution of the laser distance meter. The sample rate was 1024Hz, so that the data set is just over four minutes long and there are approximately 22.76 samples per drive period. In the results that follow, units are not typically given on the measurements since they have been scaled and transformed by the data acquisition system.

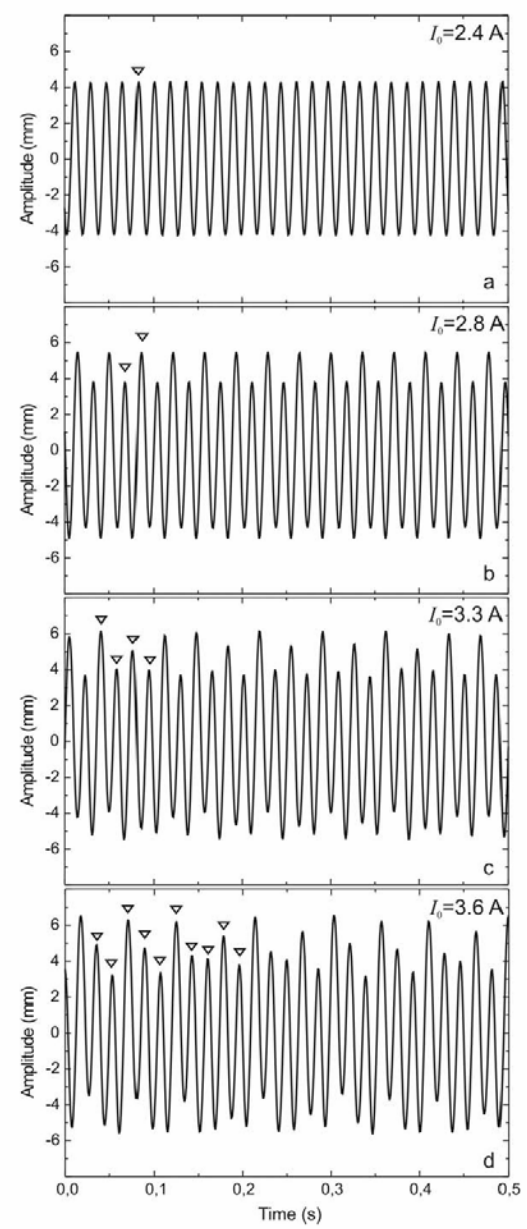

Figure 6. Short time series plots of the vibration amplitude recorded in 1 bar air for a fixed driving frequency of 56 Hz, and various driving currents. The triangles indicate the appearance of period doubling, leading to aperiodic behavior observed at 3.6A.

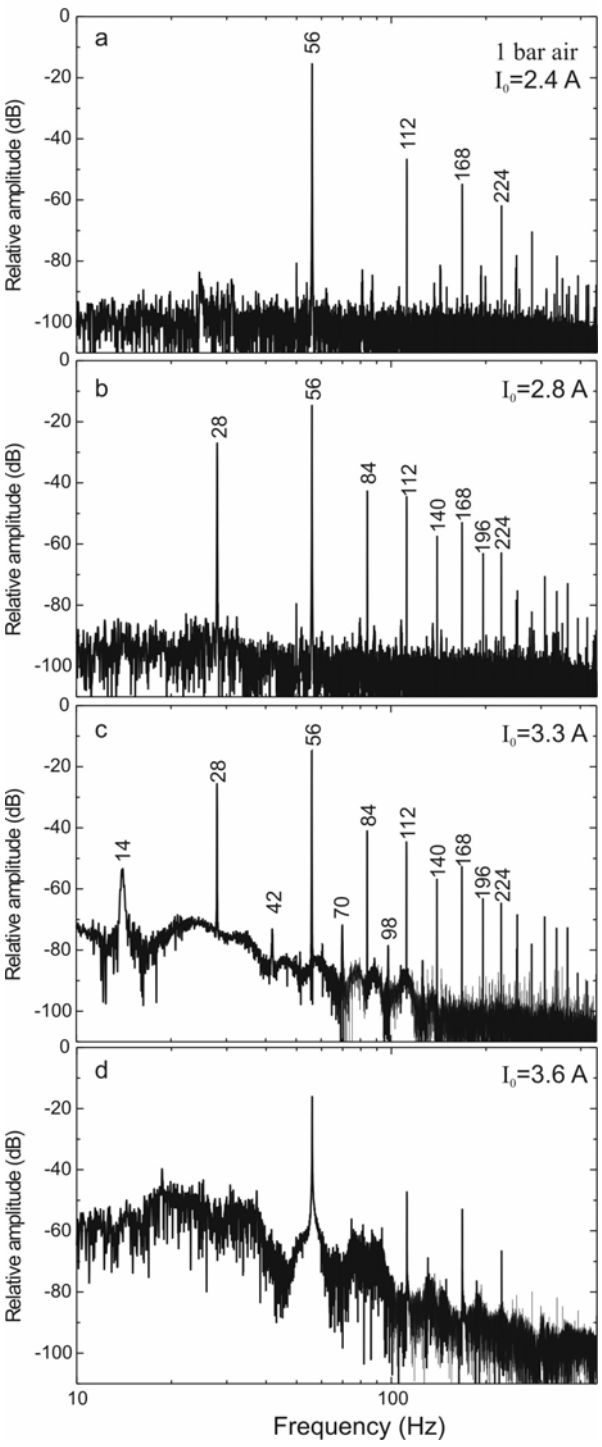

Figure 7. Average spectrum of vibration amplitude recorded in 1 bar air for various driving currents corresponding to Figure 6.

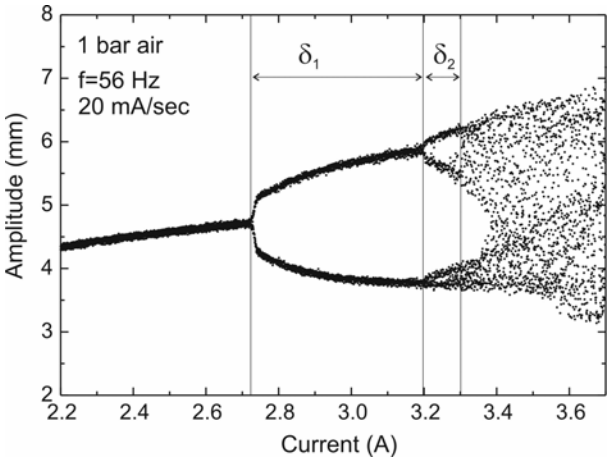

Figure 8. A bifurcation diagram of vibration amplitudes recorded in 1 bar air for a driving current swept at 20 mA/sec and fixed driving frequency of 56 Hz.

3. DATA ANALYSIS AND RESULTS

To analyse a 1 dimensional experimental data set using chaotic time series analysis techniques, it is necessary to transform the data using phase space reconstruction techniques. If only one variable from the system can be observed, $\mathbf{X}=\{X(1), X(2), ...X(N),...\}$, then a D-dimensional time series of length N, $\mathbf{Y}=\{Y(1), Y(2), ... Y(N)\}$ is constructed from the original time series using a delay d as follows.

$$\mathbf{Y}(n) = \left(X(n), X(n+d), ...X(n+(D-1)d) \right) \qquad (4)$$

where we have assumed that $\mathbf{X}$ contains at least $N+(D-1)d$ data points. If the time between samples represents one period of data, then $\mathbf{X}$ represents time series generated from a map, or Poincare section of the system. In which case the delay d used to generate $\mathbf{Y}$ is usually set to 1.

Assuming that the time series is stationary, that is, the parameters which govern the dynamics are not significantly changing over time, then with sufficient data and the appropriate choice of the delay parameter d and the embedding dimension D, $\mathbf{Y}$ will accurately represent the dynamical behaviour of the system. Once $\mathbf{Y}$ has been constructed, then further analysis of this multidimensional time series may be used to estimate various quantities related to the structure of the phase space, such as the dimensionality of the attractor, characterisation of the chaotic behavior or lack thereof, and identification of chaotic orbits.

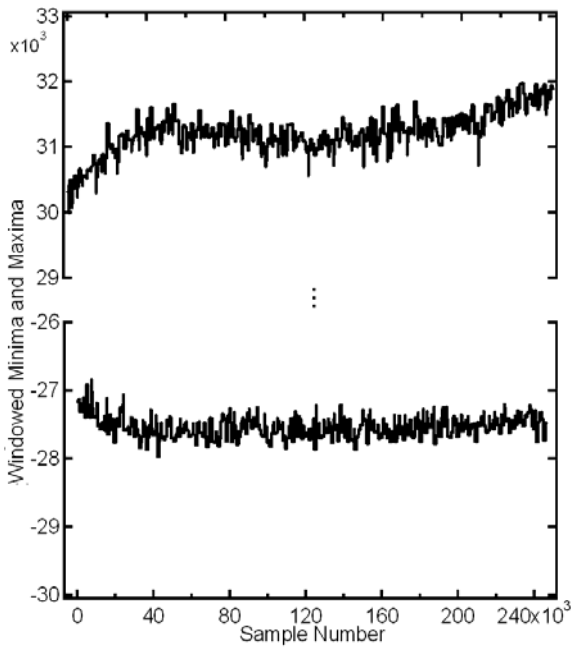

Figure 9. Nonstationary behavior of the time series. Plotted are estimates of the maximum and minimum values for overlapping windows of 1024 samples (one second) from the experimental data.

In the following subsections, we construct delay coordinate embeddings from the scalar time series, and then use this technique to analyse the data and quantify its dynamical system properties. We will use the notation introduced above to describe the original scalar time series, $\mathbf{X}=\{X(1), X(2), \ldots X(N)\}$ and a delay coordinate embedding of the time series, $\mathbf{Y}=\{Y(1), Y(2), \ldots Y(N)\}$.

3.1. Nonstationarity and long-term dynamics

A few simple tests were first performed that would identify strong drifts in the data. Sliding windows of varying length were applied to the data and statistical quantities such as mean, maximum, minimum and standard deviation were computed for each window. If the data was truly stationary, then these quantities would remain constant throughout the data. Results of the drift in the maximum and minimum values of a one second window (1024 data points) are depicted in Figure 9.

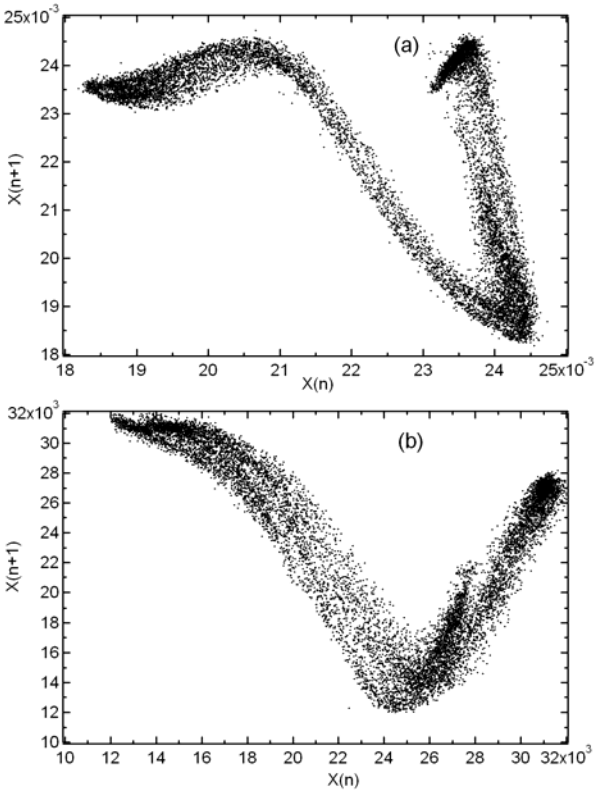

Figure 10. Plot of the waveform for two methods of sectioning the data. The top plot, part (a), depicts peak amplitudes and the bottom plot, part (b), depicts time intervals between zero crossings.

It can be seen that the dynamics of the system are not entirely stationary. For instance, the maximum value undergoes an upward trend, particularly near the beginning of the time series. This nonstationarity was also confirmed by the measurement of other statistical quantities such as the skewness and kurtosis for windowed data.

When the dynamics change over time in an experimental system it is often difficult to determine the cause. The behavior may be caused by long term dynamics which are inherent to the system or by a simple transient before settling into some behaviour. However, this fluctuation is quite small in relation to the full extent of the data (for instance, variation in the maximum value is less than 2% the full scale of the data) and thus, though it may affect the results of chaotic time series analysis methods, it is still small enough that the data is acceptable for analysis.

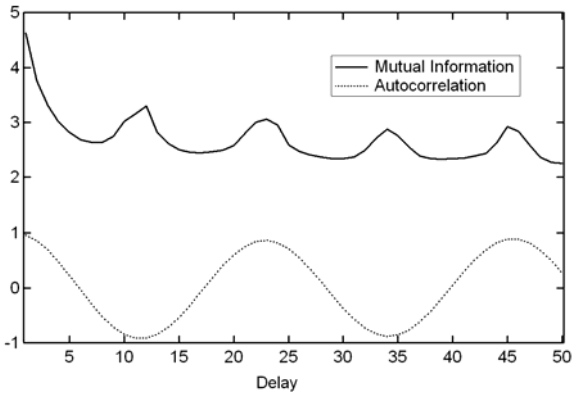

Figure 11. Two techniques for estimating an embedding delay from the experimental data. The first method uses the first minimum of the mutual information function and the second uses the first zero crossing of the autocorrelation function. The methods suggest a delay between 6 and 7.

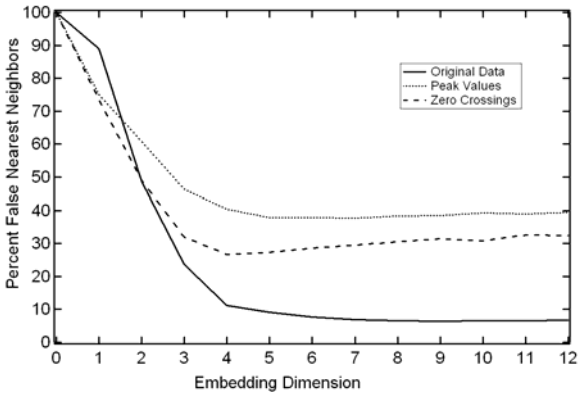

Figure 12. Results of the FNN routine as applied to the original flow data and the two Poincare sections. An appropriate embedding dimension is found when the percentage of false near neighbors drops to a constant value. This indicates that the embedding dimension should be at least 4.

3.2. Poincaré sections

A common technique in chaotic time series analysis is to generate a Poincare section, with one point per period, from data sampled at much higher than the drive frequency. Given that the system has a drive frequency of 45Hz, a natural Poincaré section would be to sample the system at the drive frequency. Since this was not possible due to the limited sampling frequencies of the data acquisition system, we considered several techniques for extracting a Poincaré section. These included the peak amplitude values, their second derivatives, times between peaks and times at which the amplitudes cross a fixed value. Figure 10 depicts the Poincare section plots using extracted peak amplitudes and extracted times between zero crossings in the flow data. Both techniques successfully capture the dynamics, though the use of zero crossings appears slightly less noisy.

3.3. Embedding parameters

A reasonable value for the delay may be suggested either by the first zero crossing of the autocorrelation function or by the first minimum of the mutual information function[18, 19], as either value is plotted as a function of delay. For the time series data, given a delay *d*, the autocorrelation is found simply from

$$R(d) = \frac{1}{(N-k)\sigma^2}\sum_{n=1}^{N-k}[X(n)-\mu][X(n+d)-\mu] \qquad (5)$$

where μ is the mean and σ^2 is the variance of the data.

The mutual information of two random variables, $a \in A$ and $b \in B$, is given by

$$I(A;B) = \sum_{a\in A}\sum_{b\in B} p(a,b)\log\frac{p(a,b)}{p(a)p(b)} \qquad (6)$$

where the convention 0log0=0 was used. In the case of the mutual information between a time series and a delayed version of itself, *a* represents a range of values for $X(n)$ and *b* a range of values for $X(n+d)$. These values must be chosen so as to provide a reasonable approximation to the mutual information of the underlying dynamical systems generating $X(n)$ and $X(n+k)$. Here, the mutual information was calculated efficiently using a method described in Reiss, et al.[20], which partitions the range of values for $X(n)$ and $X(n+k)$ recursively until there is no more hidden structure.

The mutual information often gives a better value because it takes nonlinear correlations into account. However, for the loudspeaker data, the mutual information function and the autocorrelation function were in strong agreement. As shown in Figure 11, the autocorrelation suggests a delay of 6 and the mutual information a delay of 7. This was in agreement with

visual inspection since 2 and 3 dimensional plots revealed the most structure near these values of delay (see Figure 13). Unfortunately, they also reveal a complexity or noise dependence that makes the fine scale structure very difficult to detect.

A modified form of the false nearest neighbors algorithm[21] (FNN) was chosen as the primary technique for determining the embedding dimension. The modification is intended to take into account stochastic phenomena which result in FNNs occurring regardless of the embedding dimension. An appropriate embedding dimension is found when the percentage of FNNs drops to a constant value. As shown in Figure 12, the percentage of false neighbors approaches a constant value with an embedding dimension of 5 for the flow data, and an embedding dimension of 4 for either sectioned data set. This is in agreement with the observation that a Poincaré section should have one less dimension than the original data.

3.4. Fractal dimension

The dimensionality of a chaotic attractor is typically a noninteger value. That is, the attracting region of the phase space will not completely fill out a region of that space. In this section we use several different methods to estimate the dimensionality of the loudspeaker data, which further gives an idea of the complexity of the underlying dynamics.

The correlation dimension is found by constructing a function $C(\varepsilon)$ that is the probability that two arbitrary points from the delay coordinate embedding are closer together than a distance ε.

$$C(\varepsilon) = \frac{2}{N(N-1)} \sum_{i=1}^{N} \sum_{j=1}^{i-1} H(\varepsilon - |Y(i) - Y(j)|) \qquad (7)$$

where H is the Heaviside unit step function. The correlation dimension of an experimental time series is then given by

$$D = d\log(C) / d\log(\varepsilon) \qquad (8)$$

in the limit $\varepsilon \to 0$, and $N \to \infty$. The correlation dimension may be estimated by the slope of the curve $\log(C(\varepsilon))$ versus $\log(\varepsilon)$. A noninteger result for the correlation dimension indicates that the data is probably fractal. For too low or too high ε values, the results are inaccurate, so the slope must be measured in the midrange of the curve. A good value should be in the region where measurements of the dimension are most stable.

The Grassberger-Proccacia algorithm[22, 23] was used to estimate fractal dimension. Results of $\log_2(C(\varepsilon))$ versus $\log(\varepsilon)$ for the peak values from the original 45Hz data are depicted in Figure 14. The correlation dimension cannot be accurately estimated since there is not a significant region where the slope remains constant. This is because estimates of correlation dimension using the Grassberger-Proccacia algorithm are highly susceptible to noise and data set size. Limited data set size reduces the region of the plateau and increases uncertainty, and the presence of noise implies that accurate measurement can only be obtained for large ε. For higher dimensional data these problems are aggravated since minimal noise and exponentially more data are required to identify the plateau region. In addition, data with a high sample rate may exhibit strong correlations that skew the estimates. The approximations due to noise, data set size, nonstationarity and so on are inherent in the data set. But the Grassberger-Proccacia algorithm also uses an approximation to the definition of correlation dimension. Therefore, we attempted an alternative technique that allows estimation of multiple definitions of the fractal dimension.

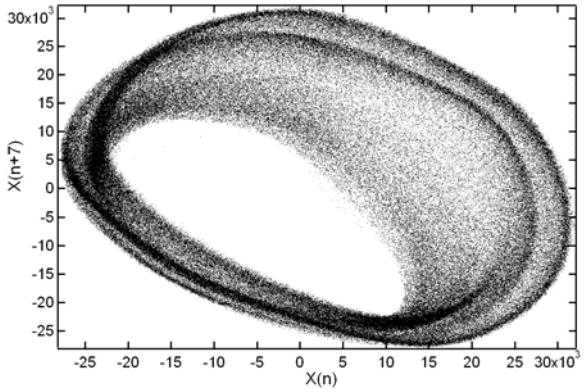

Figure 13. A two dimensional plot of the experimental data with a delay of 7.

The delay coordinate embedded data can be gridded into n-dimensional boxes of equal length ε, such that all vectors lie within these N boxes. If a box is labelled i, then it has an associated probability, $P_i(\varepsilon)$, that a vector on the attractor will reside within this box. The generalized entropies, H_0, H_1, … are defined in terms of

the probabilities of vectors occupying boxes. For q=0,1,2…,

$$H_q(\varepsilon) = \frac{1}{1-q} \ln \sum_{i=1}^{N(\varepsilon)} P_i^q(\varepsilon) \ldots q \neq 1$$
$$H_1(\varepsilon) = -\sum_{i=1}^{N(\varepsilon)} P_i(\varepsilon) \ln P_i(\varepsilon) \quad (9)$$

In the following we keep the conventions common in dimension definitions and use the natural logarithm as opposed to the log base 2. The generalized dimension of order q is then defined as

$$D(q) = -\lim_{\varepsilon \to \infty} \frac{H_q(\varepsilon)}{\ln \varepsilon} \quad (10)$$

Under this definition, $D(0)$, $D(1)$, and $D(2)$ are the box counting dimension, the information dimension and the correlation dimension, respectively. We also have the property that if $p>q$, then $D(p) \leq D(q)$.

Once the generalized entropies have been determined, there are two ways to approximate the generalized dimensions for time series data. The first is if ε is sufficiently small such that the limit is approximately correct, and we have enough data to get an accurate measurement for $H_q(\varepsilon)$. In which case we may use

$$D(q) \approx D_q(\varepsilon) = -H_q(\varepsilon) / \ln \varepsilon \quad (11)$$

However, the preferred method is to simply look at the slope of a plot of $H_q(\varepsilon)$ vs $\ln(\varepsilon)$, since this has a quicker rate of converge to the limit of ε–>0. We should mention that further information theoretic properties can be determined from the analysis of this sorting, such as the generalized mutual information of high dimensional data, $I_n(X_1,X_2,\ldots X_n)$, or estimation of the metric entropy[24].

For large box size, the box counting dimension varies widely from the others, since the box counting dimension $D(0)$ is more susceptible to errors. It is also a poor quantity to use since it says nothing about the density of the attractor, only about its shape. However, the box counting dimension and all the others converge in the mid-region, before diverging slightly and then dropping to zero (due to data set size). It is this mid region that parallels the plateau region of the Grassberger-Proccacia algorithm[22, 23].

Figure 15 and Figure 16 presents the results of our calculations of the first four generalised dimensions performed on the flow data embedded in five dimensions and the sectioned data embedded in four dimensions, respectively. Displayed are estimates of the first four generalized entropies for varying box size. Additional tests were also performed for the embedding dimensions 3-6, and for the next four generalized entropies. The results indicated that, for $p > q$, $D(p) \leq D(q)$, which agrees with theory.

The estimates for fractal dimension were derived from where the slope of of $H_q(\varepsilon)$ vs $\ln(\varepsilon)$ showed the least deviation for successive values of ε ($\varepsilon=2^{-4}$ and 2^{-5}). Estimates ranged from 1.8 to 2.2, for all fractal dimensions calculated on the sectioned data, and 2.6 to 3.0 for all fractal dimensions calculated on the flow data, when embedding dimension was greater than or equal to 4. In both cases the estimate This agrees with our choice of the embedding dimension, and is also in rough agreement with the result from the Grassberger-Proccacia algorithm. However, in general, the dimensionality of the sectioned data is less than 1 plus the dimensionality of the flow data. This may be accounted for primarily by the small data set size for the sectioned data (approximately 10,000 points), which is known to cause a slight overestimation of fractal dimension, and the relatively high sample rate of the flow data, which skewed estimates downwards[25].

3.5. Lyapunov exponents

The Lyapunov exponents characterize how chaotic a system is. For a D-dimensional dynamical system, consider the infinitesimally small D-sphere centered around a point on the attractor. As this evolves, the sphere will become an D-ellipsoid due to the deforming nature of the attractor flow. Then the i^{th} Lyapunov exponent is defined in terms of the exponential growth rate of the i^{th} principal axis of the ellipsoid.

$$\lambda_i = \lim_{t \to \infty} \frac{1}{t} \ln \frac{p_i(t)}{p_i(0)} \quad (12)$$

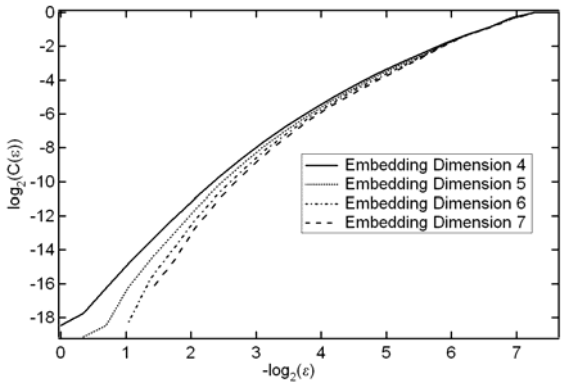

Figure 14. Plot of the log correlation function versus log distance. With sufficient, low noise data, the slope of the plot may provide the correlation dimension.

Thus the spectrum of Lyapunov exponents, $\{\lambda_1, \lambda_2, ..., \lambda_D\}$ describes the rate of growth of the distance between nearby trajectories in phase space. Chaos is often defined by the existence of a positive dominant Lyapunov exponent, which indicates that nearby trajectories will, over time, diverge exponentially away from each other.

The determination of Lyapunov exponents from noisy, experimental data is a difficult task. Although many methods have been presented, there are also numerous examples of these methods breaking down when tested against real data, as well as questions concerning the validity of the methods. Thus the results of exponent determination were held to scrutiny. Criteria were established for identification of Lyapunov exponents.

There should be agreement between exponents as measured from different algorithms, and some measurement of error should be provided. Embedding parameters used in estimating exponents must be confirmed independently by other methods. The results should remain consistent under various parameter settings for exponent estimation. For flow data, a zero exponent should be clearly found. Estimation of exponents from each both flow and sectioned data should be in agreement. The sum of all the exponents must be negative, and the sum of the positive exponents should be less than or equal to the metric entropy. In fact, for many cases they should be equal.[26] Under the proper conditions, the Lyapunov exponents should all, approximately, switch sign when measured from a time reversal of the data.[27]

The Lyapunov dimension may be defined as

$$D_\lambda = L + \frac{1}{|\lambda_{L+1}|}\sum_{j=1}^{L}\lambda_j \qquad (13)$$

where L is the maximum integer such that the sum of the L largest exponents is still non-negative. That is, $\sum_{j=1}^{L}\lambda_j \geq 0$, and $\sum_{j=1}^{L+1}\lambda_j < 0$. The Kaplan-Yorke conjecture[28] proposes that this is equal to the information dimension. Within error bounds, this seems to be true. Therefore, a final criterion is that the Lyapunov dimension estimates should agree with information dimension estimates.

It is doubtful that all criteria can be satisfied unless one is dealing with a long, noise-free time series of low dimensional simulated data. Noise, high dimensionality and short time series length (few orbits or small number of points or both) negatively affect all methods of analysis. Some criteria, such as confirmation of embedding parameter choices are a virtual necessity before any calculation is made. Others, such as agreement between the Lyapunov dimension and information dimension, are very strong indicators that Lyapunov exponents have been reasonably determined. Still other criteria require calculations of quantities that are particularly difficult to compute from time series, such as metric entropy. Previous authors chose to reject the use of estimated Lyapunov exponents as discriminating statistics[29].

Three methods of determining Lyapunov exponents were implemented; the method of Eckmann and Ruelle[30] for determining the Lyapunov spectra, and the Rosenstein[31] and Wolf, et al.,[32] methods for determining the largest exponent. Since these methods are fundamentally different, one would not expect agreement between the estimates to be simply due to them incorporating the same mistakes. The sectioned data were used for all estimates since this reduces dependence on the choice of delay time. Abarbanel's method was also applied[33], though this is based on the same technique as Eckmann and Ruelle's method and for sectioned data provides very similar results.

Wolf[32] defined the exponents in terms of the rates of divergence of volumes as they evolve around the attractor. The Wolf method involves following a trajectory in its path around the attractor. The rate of growth between points on this trajectory and a nearby trajectory is used to estimate the largest Lyapunov

exponent. When the distance between these trajectories becomes too large, then a new nearby trajectory is found that is within a reasonable angular distance from the previous nearby trajectory. In order to minimize parameter dependence, we used a variation on the Wolf method[25]. In previous work,[32, 34, 35] both maximum allowable displacement and maximum angular displacement were left as free parameters. We use one parameter: the number of near neighbors to consider after a given number of iteration steps.

The Rosenstein method involves looking at average divergence rates of nearest neighbors. It also finds the dominant exponent. The Eckmann and Ruelle method involves using a small neighborhood of points and iterating them forward to estimate the local Jacobian, and then determining the Lyapunov spectrum from the eigenvalues of the Jacobians around the attractor.

In Table I, results of exponent calculations are provided. All calculations were performed with a time delay of 1, and embedding dimension of 4, as suggested by the False Nearest Neighbors routine. The exponents are given in units of 1/time, where the time scale is defined so that the time between samples is 1. Many more calculations were performed until a reasonable and stable parameter regime was found for all methods. In general, exponent calculations converged to within 5% of their final value when averaging local estimates of the dominant Lyapunov exponent over only 1,000 points (although the entire sectioned data set was used to find near neighbors).

Table I. Results of estimation of the lyapunov exponent(s) using three different techniques. All calculations were performed with a four dimensional embedding of the peak values data.

Algorithm	λ_1	λ_2	λ_3	λ_4	**Sum**
Rosenstein	0.403				
Wolf	0.391				
Eckmann-Ruelle	0.380	0.054	-0.184	-0.484	-0.234

Several of our criteria are determined immediately upon inspection. The dominant exponent results from all three methods provide rough agreement. One check on the Wolf algorithm was calculating the average angular displacement. This was typically less than 20%, well within reasonable bounds. For the Lyapunov spectrum, the second exponent is very close to zero and the sum of the exponents is negative.

The folding of the attractor brings diverging orbits back together. So any effects of nonlinearities will most likely serve to move all exponents closer to zero. Also increasing the number of near neighbors used may underestimate the value because this allows a larger distance between neighbors. Hence a slight underestimate of the positive exponents for the Eckmann-Ruelle algorithm (and for Abarbanel's technique[33]) was expected. For the Wolf algorithm, the angular displacement errors are not likely to accumulate, but each error may skew the largest positive exponent downwards. These assumptions are confirmed by the slightly lower estimate of dominant exponent for the Eckmann-Ruelle and Wolf algorithms as compared to Rosenstein's technique, which is less susceptible to these errors.

However, it was not possible to confirm all criteria. Measurement of the metric entropy is still ongoing work. Sectioning the data introduced additional noise. More importantly, the uncertainty in sample values tended to dominate over the divergence on a small time scale, thus introducing errors into measurement of Lyapunov exponents from the original flow data. Thus it was not possible to get agreement between exponent estimates from the section and from the flow, nor was it expected. For measurement of the Lyapunov spectrum, uncertainty in the values of other exponents meant that it was not possible to get a reliable estimate of the Lyapunov dimension. Time reversal results were also inconclusive at best. However, simulated data with the addition of noise would not usually switch the signs of the exponents under time reversal either. So the sign change of exponents when the data is reversed may not be a suitable criterion for noisy data.

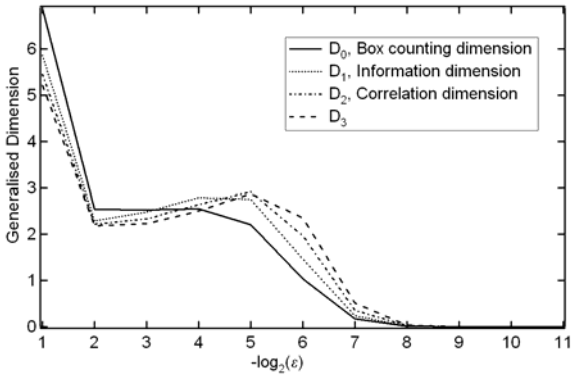

Figure 15. Plot of the first four generalized dimensions from the original data .

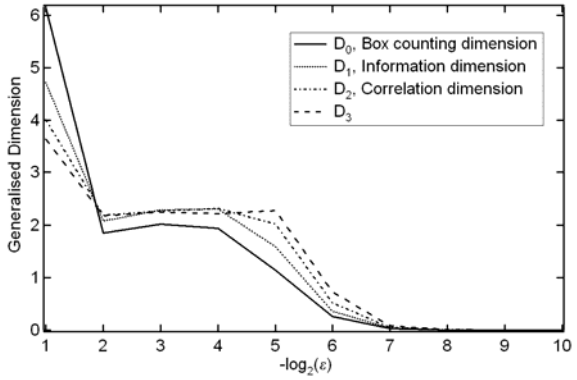

Figure 16. Plot of the first four generalized dimensions from the sectioned data.

3.6. Unstable periodic orbits

In addition to the occurrence of a positive Lyapunov exponent, a chaotic system may also be characterized by having an infinite number of unstable periodic orbits (UPOs). The identification of unstable periodic orbits plays a critical role in many chaos control algorithms[36]. Most standard chaos control algorithms attempt to control the system onto a UPO while operating within the chaotic regime. Small time-dependent perturbations applied to an accessible parameter may then be used to force the system onto the stable manifold and hence enforce stability and periodic behavior. The drive frequency is the most preferable candidate to use as the varied parameter in a control scheme. This is because it is easily adjustable and a small change in drive frequency often yields appropriate changes in the dynamics. it is useful in occasional proportional feedback control schemes, tracking and targeting of trajectories, and in the identification of symbolic dynamics[36, 37]. Thus we will also attempt to characterize the UPOs exhibited during the chaotic state.

By looking for when the dynamics approach the same region after a given number of iterates, periodic orbits can be found. UPOs of period p are found simply by establishing a threshold ε,

$$\| Y(n) - Y(n+p) \| < \varepsilon \qquad (14)$$

In which case, a periodic orbit exists in the vicinity of $Y(n)$ and a least squares fit of all data in the region can be used to estimate its exact location. The exact value of ε may be varied depending on the size of the data set, the period p and the number of UPOs that one wishes to find. Identification of false positive UPOs may be determined using the mean squared error of the least squares fit.

Figure 17 shows the delay coordinate embedding of the Poincaré section using times between zero crossings. In this figure, we identified period 1, period 2 and period 3 orbits. From the least squares fit estimate of the local dynamics, the eigenvalues and eigenvectors corresponding to the stable and unstable manifolds can be found. For the period 1 orbit, we have a fixed point located at 0.0222 seconds, corresponding to the drive frequency of the system, 45 Hz. Its eigenvalues are 0.155 and -1.571, with corresponding eigenvectors (1,0.155) and (-0.637,1). Similar results can be obtained for other identified periodic orbits, and these results can be used to implement a chaos control technique.

4. CONCLUSIONS AND FURTHER WORK

Analysis was attempted on time series data from an experimental electrodynamic loudspeaker in order to characterize the embedding dimension, fractal dimension, the Lyapunov exponents, and the unstable periodic orbits. Results were obtained which indicate that the system is governed by low dimensional chaotic dynamics, and thus is highly amenable to control, tracking, synchronization, noise reduction and so forth. Particular care was made in verifying the presence of a positive Lyapunov exponent.

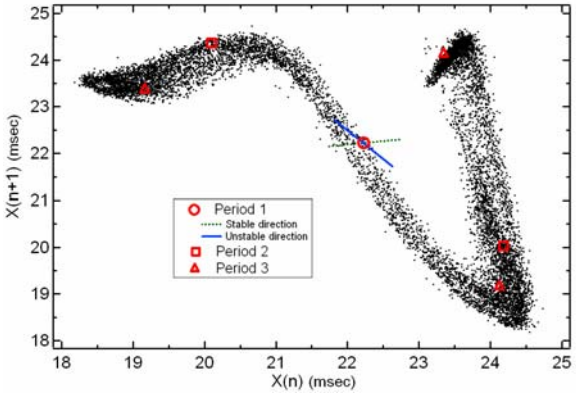

Figure 17. A delay coordinate embedding plot of the times between zero crossings. Period 1, 2 and 3 points are identified, along with the stable and unstable manifolds of the period 1 orbit.

Various estimates of fractal dimension were performed, including measurement of correlation dimension[22, 23], information dimension, and box counting dimension for different embedding dimensions. Although there was qualitative confirmation of low dimensional behavior, consistent results for quantitative values for the fractal dimension were not achieved.

However, estimation of the dominant Lyapunov exponent, which is less reliant on large data set size, provided consistent results regardless of the method of estimation[26]. Several different techniques were used which provided rough agreement in their estimates of the dominant exponent, and the results further agreed with theory concerning the Lyapunov spectrum its properties. They reliably showed evidence of a positive Lyapunov exponent, a strong indicator of chaos.

Finally, we attempted to estimate the eigenvalues and eigenvectors associated with detected unstable periodic orbits. These may be easily identified. Control may be applied to allow the loudspeaker to operate as desired within the chaotic regime. Tracking and maintenance should also be possible, since the appropriate dynamics have been found for the application of several well-known algorithms.

However, extraction of many empirical quantities, particularly fractal dimension, proved difficult due to a number of issues. This may be accounted for partly due to nonstationarity and short data set size. Though the original data set is over 200,000 points, it represents about 10,000 orbits. This is insufficient for effective calculation of fractal dimension in the presence of noise and long term dynamics. Furthermore, although the dynamics are somewhat stable, there is still a gradual change in various statistical quantities when examined using a sliding window through the data. This tends to distort various measurements. Longer data set size could capture the long term dynamics.

However, we believe that the difficulty in estimating some measures of nonlinear behavior and dimensionality is primarily due to low sample rates and low resolution due to limitations in the data acquisition system. First, the data was sampled at 1024 samples per second, or approximately 23 samples per period. A higher sampling rate would yield more accurate Poincaré sections. Alternatively, if the sampling data could be sampled at exactly the drive frequency, 45Hz, then this would produce a natural Poincaré section. The analysed data had 16 bit precision, but this was further limited by the 8 bit resolution of the A/D converter of the laser distance meter. This meant that there was significant uncertainty in the location of nearby points. Since most analysis of chaotic time series relies on analysis of near neighbors in a locally linear region, this resulted in inaccuracies in estimation of fractal dimension and Lyapunov exponents.

Current work is focused on improvements to the data acquisition system. This would allow more accurate analysis of the data, including measurements of how fractal dimension and Lyapunov dimension change with parameter settings, and use of chaotic time series prediction methods on the data. This could also be used for further direct comparison with dynamical behavior from enhanced models of the loudspeaker. An accurate model of an electrodynamic loudspeaker would represent a significant advance in the field, particularly since model parameters could then be modified to yield a loudspeaker design with optimal performance.

The investigators are also devising experimental conditions for the control of chaos[36] in the loudspeaker. In addition to more practical applications, such as robust operation of the loudspeaker in the chaotic regime, this work can be useful for composing fractal music[38]. Unlike other chaotic dynamic systems, loudspeaker operate in two-dimensions by changing two input parameters, frequency and driving current. So, the necessary two-dimensional patterns provided for successful composing can be created by two variables. Similar to other composing instruments, the loudspeaker may be used in both roles simultaneously, as a composing and music reproduction device. This is an advantage over the usual theory of fractal composing which assumes complicated interpolating electronic stages based upon synthesizers.

5. REFERENCES

[1] P. Klipsch, "Loudspeaker distortion," Proceedings of the IEEE International Conference on Acoustics, Speech, and Signal Processing, ICASSP '76, Philadelphia, PA, pp. 543- 546.

[2] R. J. Wei, Q. T. Tao, and W. S. Ni, "Bifurcation and chaos of direct radiation loudspeaker," *Chinese Phys. Lett.*, vol. 3, pp. 469-472, 1986.

[3] P. Tong, G. Miao, W. Ni, and R. Wei, "Lyapunov Exponents and General Dimensions of Strange Attractor of Electrodynamic Cone Loudspeaker," *Chinese Physics Letters*, vol. 8, pp. 442-445, 1991.

[4] D. Djurek, I. Djurek, and A. Petosic, "Intrinsic Membrane Friction and Onset of Chaos in an Electrodynamic Loudspeaker," Proceedings of the 123rd Aes Convention, New York, NY, 2007.
[5] I. Djurek, A. Petosic, and D. Djurek, "Chaotic state in an electrodynamic loudspeaker controlled by gas pressure," Proceedings of the 153rd ASA meeting, Salt Lake City, USA, 2007.
[6] D. Djurek, I. Djurek, and A. Petosic, "Chaotic State in an Electrodynamic Loudspeaker," Proceedings of the 122nd Convention of the AES, Vienna, Austria, 2007.
[7] G. Miao, W. Ni, Q. Tao, Z. Zhang, and R. Wei, "Bifurcation, chaos and hysteresis in electrodynamic cone loudspeaker," *Chinese Physics Letters*, vol. 7, pp. 68-71, 1990.
[8] H. D. I. Abarbanel, *Analysis of observed chaotic data*. New York: Springer, 1996.
[9] H. Kantz and T. Schreiber, *Nonlinear Time Series Analysis*. Cambridge, UK: Cambridge Univ. Press, 1997.
[10] M. Colloms, *High Performance Loudspeakers*, 6th ed: John Wiley & Sons, Ltd, 2005.
[11] L. D. Landau and E. M. Lifshitz, *Fluid Mechanics*, vol. 6, 2nd ed: Elsevier, 2004.
[12] I. Djurek, A. Petosic, and D. Djurek, "Mass nonlinearity and intrinsic friction of the loudspeaker membrane, Convention paper 7075," Proceedings of the 122nd AES Convention, Vienna, Austria, 2006.
[13] W. Klippel, "Dynamical Measurement of Loudspeaker Suspension Parts, Convention paper 6179," Proceedings of the 117th AES Convention, San Francisco, USA, 2004.
[14] H. Kantz and T. Schreiber, *Nonlinear Time Series Analysis*: Cambridge University Press SE - Cambridge Nonlinear Science Series, 2004.
[15] I. Djurek, D. Djurek, and A. Petosic, "Damping of an electrodynamic loudspeaker by air viscosity and turbulence," Proceedings of the 123rd Convention of Audio Engineering Society, New York, USA, 2007.
[16] T. Y. Li and J. A. Yorke, "Period three implies chaos," *Am. Math. Monthly*, vol. 82, pp. 985-992, 1975.
[17] M. J. Feigenbaum, "The universal metric properties of nonlinear transformations," *J. Stat. Phys.*, vol. 21, pp. 669-706, 1979.
[18] A. M. Fraser, "Reconstructing Attractors from Scalar Time Series: A Comparison of Singular System and Redundancy Criteria," *Physica D*, vol. 34, pp. 391-404, 1989.
[19] A. M. Fraser and H. L. Swinney, "Independent coordinates for strange attractors from mutual information," *Phys. Rev. A*, vol. 33, pp. 1134-1140, 1986.
[20] J. D. Reiss, N. Mitianoudis, and M. B. Sandler, "Computation of Generalized Mutual Information from Multichannel Audio Data," Proceedings of the Audio Engineering Society 110th Convention, Amsterdam, The Netherlands, 2001.
[21] M. B. Kennel, R. Brown, and H. D. I. Abarbanel, "Determining embedding dimension for phase-space reconstruction using a geometrical construction," *Phys. Rev. A*, vol. 45, pp. 3403-3411, 1992.
[22] P. Grassberger and I. Procaccia, "Measuring the strangeness of strange attractors.," *Physica D*, vol. 9, pp. 189-208, 1983.
[23] P. Grassberger and I. Procaccia, "On the characterization of strange attractors," *Phys. Rev. Lett.*, vol. 50, pp. 346-349, 1983.
[24] A. M. Fraser, "Information and entropy in strange attractors," *IEEE Trans. Information Theory*, vol. 35, pp. 245-262, 1989.
[25] J. D. Reiss, "The Analysis of Chaotic Time Series," PhD Thesis, *School of Physics*. Atlanta: Georgia Institute of Technology, 2001, pp. 250.
[26] J. P. Crutchfield and N. H. Packard, "Symbolic dynamics of noisy chaos.," *Physica D*, vol. 7, pp. 201, 1983.
[27] U. Parlitz, "Identification of true and spurious Lyapunov exponents from time series," *Int. J. of Bifurcation and Chaos*, vol. 2, pp. 155-165, 1992.
[28] P. Constantin and C. Foias, "Global Lyapunov exponents, Kaplan-Yorke formulas and the dimension of attractors for 2D Navier-Stokes equations.," *Commun. Pure Appl. Math.*, vol. 38, pp. 1-27, 1985.
[29] J. Theiler, S. Eubank, A. Longtin, B. Galdrikian, and J. D. Farmer, "Testing for nonlinearity in time series: the method of surrogate data," *Physica D*, vol. 58, pp. 77-94, 1992.
[30] J.-P. Eckmann, S. O. Kamphorst, D. Ruelle, and S. Ciliberto, "Liapunov Exponents from Time Series," *Phys. Rev. A*, vol. 34, pp. 4971-4979, 1986.
[31] M. T. Rosenstein, J. J. Collins, and C. J. De Luca, "A practical method for calculating largest Lyapunov exponents from small data sets," *Physica D*, vol. 65, pp. 117-134, 1993.
[32] A. Wolf, J. B. Swift, H. L. Swinney, and J. A. Vastano, "Determining Lyapunov exponents from a time series.," *Physica D*, vol. 16, pp. 285-317, 1985.
[33] H. D. I. Abarbanel, "Tools for the analysis of chaotic data," in *Nonlinear Dynamics and Time Series*, vol. 11, *Fields Inst. Communications*, C. D. Cutler and D. T. Kaplan, Eds. Providence, Rhode Island: American Math. Soc., 1997, pp. 1-16.
[34] A. Wolf, "Quantifying chaos with Lyapunov exponents," in *Chaos*, A. V. Holden, Ed. Manchester: University Press, 1986.

[35] A. Wolf and J. A. Vastano, "Intermediate length scale effects in Lyapunov exponent estimation," in *Dimensions and entropies in chaotic systems)*, G. Mayer-Kress, Ed. Berlin: Springer-Verlag, 1986.
[36] E. Schöll and H. G. Schuster, "Handbook of Chaos Control," 2nd ed: Wiley, 2007, pp. 849
[37] K. Mischaikow, M. Mrozek, J. Reiss, and A. Szymczak, "Construction of symbolic dynamics from experimental time series," *Phys. Rev. Lett.*, vol. 82, pp. 1144-1147, 1999.
[38] J. Fauvel, R. Flood, and R. Wilson, *Music and Mathematics, From Pythagoras to Fractals*: Oxford University Press, 2006.